Vol. 38 No. 4 Transactions of Information Processing Society of Japan Apr. 1997

Regular Paper

Recovery of Connection Relationships among Two-dimensional Objects

FENGHUI YAO,† GUIFENG SHAO,†† AKIKAZU TAMAKI† and KIYOSHI KATO†

This paper describes the recovery of connection relationships among two-dimensional objects. Two-dimensional objects can be expressed by their boundary curves. For a given set of boundary curves of objects, the dominant points of every boundary curve are detected. Then, by considering a set of dominant points as separation points, the corresponding boundary curve is segmented into partial boundary curves called curve segments. The curve segments belonging to the boundary curve of an object are then translated and rotated to match those of another object to obtain the matched curve segments. From these matched curve segments, the longest consecutive matched curve segments are detected. Based on these longest consecutive matched curve segments, the connection relationship between the two-dimensional objects is recovered. Finally, experiments are performed with real-world images, and the effectiveness of our method is confirmed.

1. Introduction

The shapes of objects play a very important role in object recognition, analysis, and classification. Research in this field can be roughly classified into four areas: (1) edge detection, (2) detection of the dominant points of boundary curve, (3) shape recognition, and (4) determination of connection relationships.

Research on the edge detection focuses on edges or contours and how to extract them precisely [2),5),8),9),11),16)], while work on dominant point detection focuses on the points of high curvature and how to detect them correctly. Many methods for this have been proposed [1),6),13),15),17),18),20),22)]. Research on shape recognition focuses on the entire shape of the boundary curve and how to identify or classify objects. Several methods have been suggested [12),14),19)]. Lastly, work on connection relationships focuses on the relationships between objects, that is, whether a part of an edge of an object can be connected with that of another. This kind of problem is often encountered in robot assembly systems and map-matching systems. To the authors knowledge, only one study of how to deal with this kind of problem has been carried out by Freeman and Garder [7)]. In the present paper, in an attempt to alleviate this deficiency, we present a method for recovering the connection relationships among objects [21)]. In our method, the boundary curves of objects are first extracted from the input image after binarization, and dominant points with high curvature are detected. Each boundary curve is then broken into a set of partial boundary curves called curve segments, by taking the dominant points as separation points. Segments of a curve of an object are matched with curve segments of other objects to obtain matched curve segments, and the longest consecutive matched curve segments are detected. Finally, the connection relationships among objects are recovered on basis of the longest consecutive matched curve segments.

The organization of the rest of this paper is as follows. In the next section, we briefly review Freeman and Garder's work, and point out an important problem with their algorithm. Section 3 introduces the symbols and notations employed in the description of our method. Section 4 gives an overview of the method. A digital implementation of our method is given in Section 5. Experimental results obtained by using real-world images are given in Section 6. The paper ends with some concluding remarks.

2. Brief Review of Freeman and Garder's Work

Freeman and Garder's algorithm for determining the connection relationships among two-dimensional objects may be briefly summarized as follows: (1) Express the objects by means of chain-encoding boundary curves, and

† Department of Electric, Electronic and Computer Engineering, Kyushu Institute of Technology
†† Department of Commercial Science, Seinan Gaguin University

find the slope-discontinuity points or curvature inflection points if very few or no slope-discontinuities exist; (2) Separate the boundary curves into a set of chainlets, each of which is likely to mate with one and only one chainlet from another set, and then compute their features; and (3) Calculate the feature separation between a given chainlet and all chainlets in the set of objects, to obtain the mating candidates.

This algorithm works well if the slope-discontinuity points can be obtained correctly. However, it is difficult to determine the slope-discontinuity points uniformly. For example, **Fig. 1** shows an example of a boundary curve of an object included in a real-world image. According to the above description, this curve should be separated into chainlets at the points marked "o", which seem to be the slope-discontinuity points. But the points marked "x" have similar properties to those marked "o", and they can also be treated as slope-discontinuity points. This gives rise to the wrong segmentation of the boundary curves, with the result that the chainlet candidates and the mating chainlet cannot be determined correctly. This is because the segmentation of a boundary curve at slope-discontinuity points is a kind of coarse segmentation.

To solve this problem, we perform fine segmentation at points with local maxima of the absolute curvature, to separate the boundary curve into boundary curve segments rather than chainlets. Owing to this fine segmentation, the features defined in Freeman and Garder's work can no longer be used. Here, we perform matching between the boundary curve segments belonging to every two different objects, and then determine the mating partial boundary curves where the two objects can be connected optimally. For convenience in describing the details of our method, we introduce some symbols and notations in the next section.

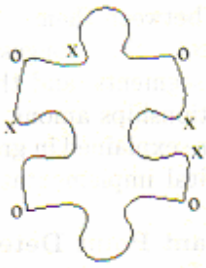

Fig. 1 Boundary curve of an object included in a real-world image.

3. Definitions, Symbols, and Notations

Before explaining the definitions, symbols, and notations, let us give two hypotheses for the target objects:

[*Hypothesis* 1] Only two-dimensional connection relationships exist among the objects; that is, the objects cannot be connected three-dimensionally.

[*Hypothesis* 2] For any three objects, there is no case in which any two of them can be connected to each other.

These two hypotheses will be used later. The remainder of this section will describe the definitions, symbols, and notations.

3.1 Two-dimensional Objects

We use O_i to denote the i-th object, and the set S_O to denote all objects, that is,

$$S_O = \{O_0, O_1, \cdots, O_{N-1}\}, \tag{1}$$

where N is the total number of objects.

3.2 Boundary Curves

For $O_i \in S_O$ $(i = 0, 1, \cdots, N-1)$, its boundary curve is denoted by C_i, which is a closed curve. In Cartesian coordinates, the boundary curve C_i is expressed by its coordinate functions $x_i(s)$ and $y_i(s)$, where s is a path-length variable along the curve (see **Fig. 2**). All boundary curves of objects in S_O are denoted by

$$S_C = \{C_0, C_1, \cdots, C_{N-1}\}. \tag{2}$$

In the following description, the boundary curve C_i is simply called curve C_i if this does not cause confusion.

3.3 Curvature

For the curve $C_i \in S_C$ $(i = 0, 1, \cdots, N-1)$, the curvature at any point M is defined as the instantaneous rate of change of α, which is the angle subtended by the tangent at point M with the X-axis, with respect to the arc-length s (see Fig. 2), given by

$$K_i(M) = \lim_{\Delta s \to 0} \frac{\Delta \alpha}{\Delta s}. \tag{3}$$

The curvature function can be defined in

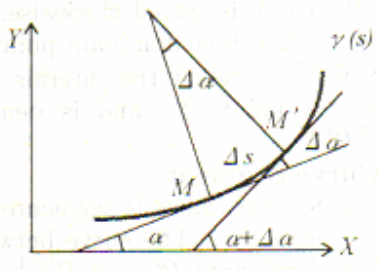

Fig. 2 Intrinsic definition of curvature.

terms of the derivative of the coordinate functions $x_i(s)$ and $y_i(s)$ as

$$K_i(x_i, y_i) = \frac{\frac{\partial^2 y_i}{\partial x_i^2}}{\left[1 + \left(\frac{\partial y_i}{\partial x_i}\right)^2\right]^{3/2}}. \quad (4)$$

A simple form of the curvature, derived by Rattarangsi and Chin [15], is cited here. Let us denote

$$\dot{x}_i = \frac{\partial x_i}{\partial s_i}, \quad \dot{y}_i = \frac{\partial y_i}{\partial s_i},$$
$$\ddot{x}_i = \frac{\partial^2 x_i}{\partial s_i^2}, \quad \ddot{y}_i = \frac{\partial^2 y_i}{\partial s_i^2},$$

then

$$\frac{\partial y_i}{\partial x_i} = \frac{\dot{y}_i}{\dot{x}_i}, \quad \frac{\partial^2 y_i}{\partial x_i^2} = \frac{\dot{x}_i \ddot{y}_i - \dot{y}_i \ddot{x}_i}{\dot{x}_i^3}.$$

Therefore, the curvature can be expressed in term of $\dot{x}_i$, $\dot{y}_i$, $\ddot{x}_i$, and $\ddot{y}_i$ as

$$K_i(x_i, y_i) = \frac{\dot{x}_i \ddot{y}_i - \dot{y}_i \ddot{x}_i}{[\dot{x}_i^2 + \dot{y}_i^2]^{3/2}}. \quad (5)$$

Furthermore, the function $x_i(s)$ and $y_i(s)$ must be related by

$$\frac{\partial x_i}{\partial s_i} = \cos\alpha, \quad \frac{\partial y_i}{\partial s_i} = \sin\alpha \quad (6)$$

which yields the curvature expression given by

$$K_i(x_i, y_i) = \dot{x}_i \ddot{y}_i - \dot{y}_i \ddot{x}_i. \quad (7)$$

$K_i(x_i, y_i)$ is also simply written as K_i, and all curvature functions of curves in S_C are denoted by

$$S_K = \{K_0, K_1, \cdots, K_{N-1}\}. \quad (8)$$

3.4 Dominant Point and the Interior Angle of the Dominant Point

A dominant point is normally considered as a point on the curve at which the absolute curvature has a maximum. For $C_i \in S_C$, its k-th dominant point is denoted by P_i^k, and all its dominant points are denoted by

$$S_{P_i} = \{P_i^0, P_i^1, \cdots, P_i^{D_i-1}\}, \quad (9)$$

where D_i is the total number of dominant points of the curve C_i. The dominant points are numbered clockwise.

When the curve is traced clockwise, the angle formed by the three dominant points P_i^{k-1}, P_i^k, and P_i^{k+1} is called the interior angle of the dominant point P_i^k, and is denoted by $\angle P_i^{k-1} P_i^k P_i^{k+1}$.

3.5 Curve Segment

For $C_i \in S_C$, the curve is segmented at the dominant points S_{P_i}. The curve between two consecutive dominants P_i^k and P_i^{k+1} is called a *curve segment*, where $k = 0, 1, \cdots, D_i - 1$ (modulo D_i). Multiple consecutive curve segments form a *partial curve*. A partial curve, when it is traced from the dominant point P_i^j to P_i^k clockwise, is denoted by C_i^{jk}, and when it is traced from P_i^k to P_i^j counterclockwise, it is denoted by $\hat{C}_i^{kj}$, where $j, k = 0, 1, \cdots, D_i - 1$ and $j \neq k$ (see **Fig. 3**). When $k = j + 1$, the partial curve becomes a curve segment.

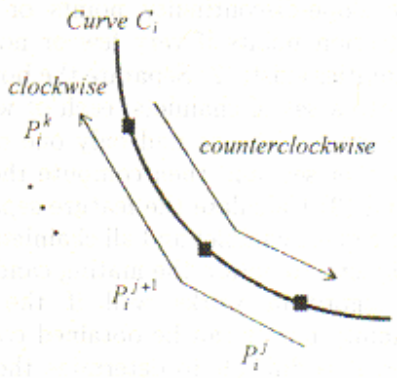

Fig. 3 Curve segment and partial curve.

All clockwise and counterclockwise curve segments of C_i are respectively denoted by

$$S_{C_i} = \{C_i^{01}, C_i^{12}, \cdots, C_i^{D_i-2,D_i-1}, C_i^{D_i-1,0}\}, \quad (10)$$

$$\hat{S}_{C_i} = \{\hat{C}_i^{10}, \hat{C}_i^{21}, \cdots, \hat{C}_i^{D_i-1,D_i-2}, \hat{C}_i^{0,D_i-1}\}. \quad (11)$$

4. Algorithm Overview

The algorithm for recovering connection relationships among two-dimensional objects can be formulated in three steps:

Step 1. Express the objects by their boundary curves, and extract the dominant points of each curve.

Step 2. Separate the curves into sets of curve segments by taking the dominant points as the separation points, perform matching between every two curve segments that belong to two different objects, and calculate the minimal matching error between them.

Step 3. Detect the longest consecutive matched curve segments, and then recover the connection relationships among objects.

These steps are explained in greater detail below. Their digital implementation is given in Section 5.

4.1 Dominant Point Detection

There have been many attempts to detect dominant points [1),6),13),15),17),18),20),23)].

Among the proposed methods, dominant point detection based on multiple-scale curvature is reliable and robust with respect to noise[15]. Therefore, we employ this method to detect the dominant points.

To express the curvature shown by Eq. (7) at varying levels of detail, both boundary coordinates functions $x_i(s)$ and $y_i(s)$ of the curve $C_i \in S_C$ are convolved with the Gaussian function $g(s,\sigma)$ defined by

$$g(s,\sigma) = \frac{1}{\sigma\sqrt{2\pi}} e^{-\frac{s^2}{2\sigma^2}}, \tag{12}$$

where σ is the standard deviation of the distribution. The Gaussian function has been used by many others to generate multiple-scale signal representations. It decreases smoothly with distance, and is differentiable and integrable. Let us assume for the time being that σ of the Gaussian function is small in comparison with the total length of the curve and that the curve in question is closed. The Gaussian-smoothed coordinate functions $X_i(s,\sigma)$ and $Y_i(s,\sigma)$ are defined by

$$X_i(s,\sigma) = \int_{u=s-\frac{S_i}{2}}^{u=s+\frac{S_i}{2}} x_i(u) g(s-u,\sigma) du, \tag{13}$$

$$Y_i(s,\sigma) = \int_{u=s-\frac{S_i}{2}}^{u=s+\frac{S_i}{2}} y_i(u) g(s-u,\sigma) du, \tag{14}$$

where S_i is the total length of the curve C_i. The limit of the integration in Eqs. (13) and (14) is to prevent the wrap-around effect of the convolving Gaussian function. In other words, the curvature function of the closed curve is assumed to be of finite duration, which avoids aliasing as a result of circular convolution in the Gaussian smoothing process if a periodic function is used. This condition is also essential to the convergence of the scale space[22], which guarantees that the number of zero crossings decreases as σ increases. Note that both $X_i(s,\sigma)$ and $Y_i(s,\sigma)$ are smooth functions, since any derivative of $X_i(s,\sigma)$ is equal to the convolution of $x_i(s)$ with a Gaussian derivative of the same order (the same thing is also true for $Y_i(s,\sigma)$). Hence, the curvature $K_i(s,\sigma)$ of a Gaussian-smoothed curve is readily given by substituting $\dot{X}_i(s,\sigma)$, $\dot{Y}_i(s,\sigma)$, $\ddot{X}_i(s,\sigma)$, and $\ddot{Y}_i(s,\sigma)$ for $\dot{x}_i$, $\dot{y}_i$, $\ddot{x}_i$, and $\ddot{y}_i$ in Eq. (7), which is rewritten as

$$K_i(s,\sigma) = \dot{X}_i(s,\sigma)\ddot{Y}_i(s,\sigma) - \dot{Y}_i(s,\sigma)\ddot{X}_i(s,\sigma). \tag{15}$$

To determine the dominant points of the curve C_i at a given scale σ, we solve for all the locations that have maxima of the absolute curvature, $|K_i(s,\sigma)|$, which are the positive maxima and negative minima of the curvature. Here, the smoothing Gaussian function was cut off (set to zero) beyond three standard deviations to have an extent of six standard deviations. This limits the scale of σ to the range from 0 to $\sigma_{\max} = S_i/6$, where S_i is the total perimeter arc length of the curve C_i. This finite-extent smoothing window satisfactorily represents the Gaussian function.

4.2 Curve Segmentation

The dominant points of $C_i \in S_C$ obtained according to the above method are given by Eq. (9), that is, $S_{P_i} = \{P_i^0, P_i^0, \cdots, P_i^{D_i-1}\}$, where D_i is the total number of dominant points. The dominant points are numbered clockwise. By considering these dominant points as the separation points, the curve C_i can be separated into curve segments. All clockwise curve segments and counterclockwise curve segments of C_i are denoted by sets S_{C_i} and $\hat{S}_{C_i}$, respectively, which are given by Eqs. (10) and (11).

Note here that the notation C_i^{mn} in Eq. (10) means a curve segment traced clockwise from the dominant point P_i^m to the dominant point P_i^n along the curve C_i, and that the dominant point P_i^m is the initium, and P_i^n the terminus of the curve segment C_i^{mn}. The notation $\hat{C}_i^{pq}$ in Eq. (11) means a curve segment traced counterclockwise from the dominant point P_i^p to the dominant point P_i^q along the curve C_i. The dominant point P_i^p is the initium, and P_i^q the terminus of the curve segment $\hat{C}_i^{pq}$.

4.3 Partial Curve Matching

Usually, a human checks whether two objects can be connected by rotating one object clockwise and the other one counterclockwise, and then bringing one object next to the other to see the gap between them. If the gap is small enough, the two objects are thought to be connectable at this orientation. Otherwise, the human will continue to rotate and match the two objects to find an orientation suitable for connection. A computer can simulate this process by using clockwise curve segments and the counterclockwise curve segments. Details are

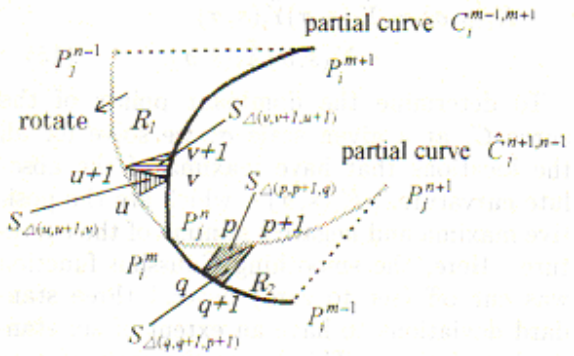

Fig. 4 Partial curve $\hat{C}_j^{n+1,n-1}$ is translated so that the dominant point P_i^m and the dominant point P_j^n overlap, and is then rotated clockwise.

given below.

For the curves $C_i, C_j \in S_C$, the clockwise curve segments of C_i and the counterclockwise curve segments of C_j are represented by Eqs. (10) and (11), namely, $S_{C_i} = \{C_i^{01}, C_i^{12}, \cdots, C_i^{D_i-2,D_i-1}, C_i^{D_i-1,0}\}$ and $\hat{S}_{C_j} = \{C_j^{10}, C_j^{21}, \cdots, C_j^{D_j-1,D_j-2}, C_j^{0,D_j-1}\}$, respectively, where D_i and D_j are the numbers of dominants points of the curves C_i and C_j, correspondingly. Matching of the curve segments $C_i^{m-1,m} \in S_{C_i}$ and $\hat{C}_j^{n+1,n} \in \hat{S}_{C_j}$ is performed through the clockwise consecutive curve segment pair $C_i^{m-1,m}C_i^{m,m+1}$ (i.e., the partial curve $C_i^{m-1,m+1}$) and the counterclockwise consecutive curve segment pair $\hat{C}_j^{n+1,n}\hat{C}_j^{n,n-1}$ (i.e., the partial curve $\hat{C}_j^{n+1,n-1}$), where $m = 0, 1, \cdots, D_i - 1$ and $n = 0, 1, \cdots, D_j - 1$ (see **Fig. 4**). First, the partial curve $\hat{C}_j^{n+1,n-1}$ is translated so that the dominant point P_j^n included in this partial curve overlaps the dominant point P_i^m included in the partial curve $C_i^{m-1,m+1}$. The displacements of X-axis and Y-axis are given by

$$D_x(C_i^{m-1,m+1}, \hat{C}_j^{n+1,n-1}) = x_i(m) - x_j(n), \quad (16)$$

$$D_y(C_i^{m-1,m+1}, \hat{C}_j^{n+1,n-1}) = y_i(m) - y_j(n), \quad (17)$$

where $(x_i(m), y_i(m))$ are the coordinates of the dominant point P_i^m of the curve C_i, and $(x_j(n), y_j(n))$ are the coordinates of the dominant point P_j^n of the curve C_j. Then, the partial curve $\hat{C}_j^{n+1,n-1}$ is rotated clockwise from 0° to 360°, in steps of δ°. The matching error is calculated after each rotation. When the partial curve $\hat{C}_j^{n+1,n-1}$ is rotated through θ°, the matching error is defined by

$$E(C_i^{m-1,m}, \hat{C}_j^{n+1,n})_\theta = \iint_{R1} dxdy + \iint_{R2} dxdy, \quad (18)$$

where R_1 is the region circled by the curve segments $C_i^{m,m+1}$ and $\hat{C}_j^{n,n-1}$ and the dotted-line $\overline{P_j^{n-1}P_i^{m+1}}$, and R_2 is the region circled by the curve segments $C_i^{m-1,m}$ and $\hat{C}_j^{n+1,n}$ and the dotted-line $\overline{P_j^{n+1}P_i^{m-1}}$ (see Fig. 4). When the partial curve $\hat{C}_j^{n+1,n-1}$ is rotated from 0° to 360° in steps of δ°, the minimal value of $E(C_i^{m-1,m}, \hat{C}_j^{n+1,n})_\theta$ is called the minimal matching error between the curve segment $C_i^{m-1,m}$ and $\hat{C}_j^{n+1,n}$. The minimal matching error is denoted as $E(C_i^{m-1,m}, \hat{C}_j^{n+1,n})_{\min}$, and the corresponding rotation angle is denoted as $\theta(C_i^{m-1,m}, \hat{C}_j^{n+1,n})_{\min}$. In the following, if there is no confusion, the parts in parentheses are omitted, and are simply denoted as $E_{\min}$ and $\theta_{\min}$. $E_{\min}$ is given by

$$E_{\min} = \min\{E_{1\delta}, E_{2\delta}, \cdots, E_{t\delta}\}, \quad (19)$$

where $t = 360/\delta$.

As above, $\forall \hat{C}_j^{n+1,n} \in \hat{S}_{C_j}$ $(n = 0, 1, \cdots, D_j - 1)$ is matched with $\forall C_i^{m-1,m} \in S_{C_i}$ $(m = 0, 1, \cdots, D_i - 1)$, and the matching error is calculated according to Eq. (18). We can obtain an $E_{\min} - \theta_{\min}$ error map. By analyzing the $E_{\min} - \theta_{\min}$ error map, we can obtain the longest consecutive matched curve segments (LCMCs), and then determine the connection relationships. Details are given in the next section.

4.4 LCMC Determination and Connection Relationship Discrimination

For the curve segment $C_i^{m-1,m} \in S_{C_i}$ and $\hat{C}_j^{n+1,n} \in \hat{S}_{C_j}$, if the following three conditions are satisfied, the curve segment pairs $C_i^{m-1,m}C_i^{m,m+1}$ and $\hat{C}_j^{n+1,n}\hat{C}_j^{n,n-1}$ are said to be "*matched*":

(1) The minimal matching error between the curve segment $C_i^{m-1,m}$ and $\hat{C}_j^{n+1,n}$ is smaller than the threshold value E_{thres}; that is,

$$E(C_i^{m-1,m}, \hat{C}_j^{n+1,n})_{\min} < E_{thres}.$$

(2) The minimal matching error between the clockwise consecutive curve segment of $C_i^{m-1,m}$ and the counterclockwise consecutive curve segment of $\hat{C}_j^{n+1,n}$ is also smaller than the threshold value E_{thres};

that is,

$$E(C_i^{m,m+1}, \hat{C}_j^{n,n-1})_{\min} < E_{thres}.$$

(3) The absolute value of the difference between the rotation angle of the curve segment $\hat{C}_j^{n+1,n}$ when it is matched with $C_i^{m-1,m}$ and the rotation angle of the curve segment $\hat{C}_j^{n,n-1}$ when it is matched with $C_i^{m,m+1}$ is smaller than the threshold value $\Delta\theta_{thres}$; that is,

$$|\theta(C_i^{m-1,m}, \hat{C}_j^{n+1,n})_{\min} - \theta(C_i^{m,m+1}, \hat{C}_j^{n,n-1})_{\min}| < \Delta\theta_{thres}.$$

Two curve segments, $C_i^{m-1,m}$ and $\hat{C}_j^{n+1,n}$, form the initium of an LCMC. Next, the focus is moved to the curve segments $C_i^{m,m+1} \in S_{C_i}$ and $\hat{C}_j^{n,n-1} \in \hat{S}_{C_j}$ and the above process is repeated. This continues until all consecutive curve segment pairs that satisfy the above three conditions are found. These consecutive matched curve segment pairs make up an LCMC. The curve segment pairs at which the repetition processing stops form the terminus of the LCMC. The number of the matched curve segment pairs in an LCMC is called the "*length*".

In this way, all possible LCMCs among the curve segments in S_{C_i} and $\hat{S}_{C_j}$ can be obtained. Let us denote these LCMCs as

$$S_{LCMC} = \{\langle C_i^{m-1,m+L_1}, \hat{C}_j^{n+1,n-L_1}\rangle, \langle C_i^{u-1,u+L_2}, \hat{C}_j^{v+1,v-L_2}\rangle, \cdots, \langle C_i^{p-1,p+L_Q}, \hat{C}_j^{q+1,q-L_Q}\rangle\} \quad (20)$$

where Q represents the total number of LCMCs, and $L_1, L_2, \cdots, L_Q$ the lengths of LCMCs, correspondingly, and $\langle \_, \_ \rangle$ denotes an LCMC that has two partial curves formed by curve segments in S_{C_i} and $\hat{S}_{C_j}$, respectively. These LCMCs are used to determine the connection relationship between the objects O_i and O_j below.

The partial curves $\hat{C}_j^{n+1,n-L_1}, \hat{C}_j^{v+1,v-L_2}, \cdots, \hat{C}_j^{q+1,q-L_Q}$ are rotated to the same inclination as the partial curves $C_i^{m-1,m+L_1}, C_i^{u-1,u+L_2}, \cdots, C_i^{p-1,p+L_Q}$, respectively, and translated so that the centers of the partial curves $\hat{C}_j^{n+1,n-L_1}, \hat{C}_j^{v+1,v-L_2}, \cdots, \hat{C}_j^{q+1,q-L_Q}$ are overlapped with those of $C_i^{m-1,m+L_1}, C_i^{u-1,u+L_2}, \cdots, C_i^{p-1,p+L_Q}$, and the matching errors of these LCMCs are then calculated according to Eq. (18). The rotation angle is defined by

$$\theta\left(C_i^{s-1,s+R}, \hat{C}_j^{t+1,t-R}\right) = arctan\left(\frac{y_{t-R} - y_{t+1}}{x_{t-R} - x_{t+1}}\right) - arctan\left(\frac{y_{s+R} - y_{s-1}}{x_{s+R} - x_{s-1}}\right), \quad (21)$$

where $s = m, u, \cdots, p$, $t = n, v, \cdots, q$, $R = L_1, L_2, \cdots, L_Q$, (x_{s-1}, y_{s-1}) and (x_{s+R}, y_{s+R}) are the coordinates of the initium and terminus of the partial curve $C_i^{s-1,s+R}$, and (x_{t+1}, y_{t+1}) and (x_{t-R}, y_{t-R}) are the coordinates of the partial curve $\hat{C}_j^{t+1,t-R}$, respectively.

In S_{LCMC}, LCMCs whose lengths are smaller than the threshold value L_{thres} are discarded. After this filtering processing, if there is more than one LCMC left in S_{LCMC}, the LCMC whose matching error is the smallest is assumed to be the part where the objects O_i and O_j can be connected optimally. If there is no LCMC whose length is greater than L_{thres}, there is no connection relationship between the objects O_i and O_j.

Note here that the value of $\Delta\theta_{thres}$ is fixed, and is determined experimentally. However, the value of E_{thres} depends on the lengths of the curve segments in comparison, and cannot be fixed. E_{thres} is dynamically determined by

$$E_{thres} = W_E \times \max\{A_i^0, A_i^1, \cdots, A_i^{D_i-1}, A_j^0, A_j^1, \cdots, A_j^{D_j-1}\}, \quad (22)$$

where A_i^m is the area of the triangle formed by the dominant points P_i^{m-1}, P_i^m, and P_i^{m+1}, A_j^n is the area of the triangle formed by the dominant points P_j^{n-1}, P_j^n, and P_j^{n+1} ($m = 0, 1, \cdots, D_i - 1$, modulo D_i, $n = 0, 1, \cdots, D_j - 1$, modulo D_j); and W_E is the weighting coefficient, which will be determined experimentally.

4.5 Recovery of Connection Relationships

In the above method, the curve segments of $\forall O_i, O_j \in S_O$ $(i \neq j)$ are matched with each other to obtain the LCMC between them. There are probably cases in which there is an LCMC between every two different objects. It is clear that not all LCMCs represent the correct connection relationships among objects. These LCMCs are filtered according to the following two rules:

[*Rule* 1] If the partial curve C_k^{ij} of object O_k matches the partial curves $\hat{C}_o^{mn}, \hat{C}_r^{pq}, \cdots, \hat{C}_w^{uv}$

of the objects $O_o, O_r, \cdots, O_w$ at the same time, where $o \neq r \cdots \neq w$, all these LCMCs are contradictory (according to *hypothesis* 1), and are discarded.

[*Rule* 2] If the partial curves C_k^{ij} and C_k^{mn} of object O_k match the partial curves $\hat{C}_t^{rs}$ and $\hat{C}_w^{uv}$ of objects O_t and O_w, respectively, and the partial curve C_t^{pq} of the object O_t matches the partial curve $\hat{C}_w^{xy}$ of object O_w, where $t \neq w$, there exists a contradictory matched partial curve among the objects O_k, O_t, and O_w (according to *hypothesis* 2). The LCMC with the biggest matching error is discarded.

Since we are discussing connection relationships among 2-D objects, *Rule* 1 is given a higher priority (refer to *hypothesis* 1). After this filtering operation, the remaining LCMCs are used to recover the connection relationship. First, the number of matched curves of each object is calculated. The object with the maximal matched curve number is selected as the base object for which the recovery of the connection relationship is performed. The base object is not rotated or translated in the recovery operation. The recovery procedure has two steps.

In the first step, objects that can be connected to the base object directly are processed. The translation along the X-axis is the difference between the x-coordinates of the center points of the two matched partial curves, and that along the Y-axis the difference between the y-coordinates. The rotation angle to the base object is calculated as shown in Eq. (21). It is worth noting that the coordinates of the object will be changed correspondingly if it is translated or rotated.

In the second step, objects that can be connected to the base object indirectly are processed. For example, if object O_i can be connected to the base object directly, and object O_j can be connected to object O_i, we say that object O_j can be connected to the base object indirectly. The displacements of object O_j along the X-axis and Y-axis can be obtained in the same way as above, because the coordinates of object O_i are changed in the first step. The rotation angle of object O_j is the sum of the rotation angle of object O_i to the base object and that of O_j to O_i. Generally, if object O_w can be connected to the base object via objects $O_k, O_p, \cdots, O_u, O_v$, the rotation angle of object O_w is the sum of the rotation angle of O_k to the base object, that of O_p to $O_k, \ldots$, and that of O_v to O_u. The experimental results will be given in Section 6.

5. Digital Implementation

5.1 Digital Dominant Point Detection

For a digital implementation, it is necessary to define the digital boundary curve, the digital curvature, and the digital matching error. Let us represent the coordinate functions $x_i(s)$ and $y_i(s)$ of the curve C_i digitally by a set of equally spaced Cartesian grid samples $\{x_i^k, y_i^k\}$ for $k = 0, 1, \cdots, S_i - 1$ (modulo S_i). The digital curvature at point k on the curve C_i is computed by

$$K_i^k = \Delta x_i^k \Delta^2 y_i^k - \Delta y_i^k \Delta^2 x_i^k, \qquad (23)$$

where Δ denotes the difference operator and Δ^2 is the second-order difference operator [15].

The digital Gaussian function in Burt's work [3] with a window size of $K = 3$ is used here to generate smoothing functions at various values of σ, and is given by

$$h[0] = 0.2261, \quad h[1] = 0.5478, \quad h[2] = 0.2261, \qquad (24)$$

where $h[1]$ is the center value and $\sum h[k] = 1$ $(k = 0, 1, 2)$. This digital function has been mentioned as the best approximation of the Gaussian distribution [4),10]. For the digital smoothing function with higher values of σ, the above $K = 3$ function is used in a repeating convolution process. For example, a $K = 5$ smoothing function is obtained by convolving Eq. (24) with itself once, and a $2(j+1)+1$ digital smoothing function is created by repeating the self-convolution process j times.

For the curve C_i digitally represented by $\{x_i^k, y_i^k\}$ for $k = 0, 1, \cdots, S_i - 1$ (modulo S_i), which has a perimeter arc length of length S_i, the digital Gaussian smoothing function with a largest σ for the coarsest boundary representation must have a window size no larger than S_i in order to avoid aliasing.

A digital multiscale representation of the curve C_i from $\sigma = 0$ to $\sigma_{\max}$ $(= S_i/6)$ is constructed by the digital Gaussian function defined above. The multiscale digital curvature of the curve C_i can be obtained according to Eqs. (23) and (24). The next step is to determine the dominant points for a given $\sigma (0 \sim \sigma_{\max})$. Details are as follows: For each point k of the curve C_i, a searching procedure is applied to detect the local maximum of the absolute curvature within the region of support

given by the sequence $\{\mid K_i^l \mid, \cdots, \mid K_i^{k-1} \mid, \mid K_i^k \mid, \mid K_i^{k+1} \mid, \cdots, \mid K_i^r \mid\}$, where K_i^k is the curvature of the point in question, and K_i^l and K_i^r are the leftmost and rightmost points of the local region of support, respectively. The region of support for each point k is the largest possible window containing k in which $\mid K_i \mid$ to both the left and right of k is strictly decreasing. A boundary point is not an absolute maximum if such a region of support cannot be determined for that point.

It is reasonable to believe that some of the detected maxima of absolute curvature do not correspond to the true dominant points of the boundary curve. Although such a point is detected numerically as the local absolute maximum, the measurable digital differences in curvature between the point and its neighbors in the region of support are very small, sometimes approaching machine precision; that is, both $\mid K_i^k \mid - \mid K_i^l \mid$ and $\mid K_i^k \mid - \mid K_i^r \mid$ are positive but approaching zero. An example of numerical absolute maxima is boundary noise on straight lines. A one-pixel boundary noise on a horizontal straight line will generate three numerical maxima of absolute curvature that persist through all scales. The difference in curvature between such an absolute maximum and other points in its region of support is very small, especially for large σ. Although these absolute maxima exist theoretically when the boundary curve is treated as a continuous function, they should not be treated as valid absolute curvature maxima in the digital implementation.

To detect a false absolute maximum, say at k, the region of support based on the curvature is first determined, as previously described. Then, the perpendicular distance from the absolute maximum at k to the line passing through the two end points at l and r of the region of support is measured. The maximum at k is considered to be a false absolute maximum if the measured distance is smaller than one pixel. This threshold is determined on basis of the fact that a slanted straight line is quantized into a set of either horizontal or vertical line segments separated by one-pixel steps. In addition, it is assumed that boundary noise is no more than one pixel, and if the noise level is known *a priori*, this threshold can be adjusted accordingly.

Moreover, if the interior angle of the dominant point P_i^w, that is, the angle formed by the dominant points P_i^{w-1}, P_i^w, and P_i^{w+1}, is greater than 170°, these three dominant points are considered to lie on the same straight line, and the dominant point P_i^w is discarded.

After the above filtering, the remaining dominant points are thought of as separation points. The curve C_i is separated into curve segments at these points. This is done to all curves in S_C.

5.2 Digital Matching Error

The matching error between the curve segments $C_i^{m-1,m} \in S_{C_i}$ and $\hat{C}_j^{n+1,n} \in \hat{S}_{C_j}$ discussed in Section 4.3 is computed digitally as follows:

$$E(C_i^{m-1,m}, \hat{C}_j^{n+1,n})_\theta = \sum_{p=0,q=0}^{\max\{P,Q\}} (S_{\Delta(p,p+1,q)} + S_{\Delta(q,q+1,p+1)}) + \sum_{u=0,v=0}^{\max\{U,V\}} (S_{\Delta(u,u+1,v)} + S_{\Delta(v,v+1,u+1)}), \tag{25}$$

where P, Q, U, and V are the lengths of the curve segments $\hat{C}_j^{n+1,n}$, $C_i^{m-1,m}$, $\hat{C}_j^{n,n-1}$, and $C_i^{m,m+1}$, respectively, and $S_{\Delta(p,p+1,q)}$, $S_{\Delta(q,q+1,p+1)}$, $S_{\Delta(u,u+1,v)}$, and $S_{\Delta(v,v+1,u+1)}$ are the areas of the triangles formed by the boundary points p, $p+1$, and q; q, $q+1$, and $p+1$; u, $u+1$, and v; and v, $v+1$, and $u+1$, correspondingly, as shown in Fig. 4. The areas of the triangles are computed as follows:

$$S_{\Delta(p,p+1,q)} = (y_j^p - y_j^{p+1})x_i^q - (x_j^p - x_j^{p+1})y_i^q + (x_j^p - x_j^{p+1})y_j^p - (y_j^p - y_j^{p+1})x_j^p, \tag{26}$$

$$S_{\Delta(q,q+1,p+1)} = (y_i^q - y_i^{q+1})x_j^{p+1} - (x_i^q - x_i^{q+1})y_j^{p+1} + (x_i^q - x_i^{q+1})y_i^q - (y_i^q - y_i^{q+1})x_i^q, \tag{27}$$

$$S_{\Delta(u,u+1,v)} = (y_j^u - y_j^{u+1})x_i^v - (x_j^u - x_j^{u+1})y_i^v + (x_j^u - x_j^{u+1})y_j^u - (y_j^u - y_j^{u+1})x_j^u, \tag{28}$$

$$S_{\Delta(v,v+1,u+1)} = (y_i^v - y_i^{v+1})x_j^{u+1} - (x_i^v - x_i^{v+1})y_j^{u+1} + (x_i^v - x_i^{v+1})y_i^v - (y_i^v - y_i^{v+1})x_i^v. \tag{29}$$

Note that if a curve segment has fewer points

than the one it is being compared with, its initium or terminus will be used to correspond to the left point of the curve segment it is being compared with, in order to continue the calculation in Eqs. (25)–(29). Which one will be used is determined by the tracing direction along the curve segment. For example, in the region R_2 in Fig. 4, the calculation starts from the overlapping dominant point P_i^{m-1} (that is, P_j^n). The matching error is calculated by taking one point from each curve segment $C_i^{m-1,m}$ and $\hat{C}_j^{n+1,n}$, and substituting it into the first item of Eq. (25). Because the curve segment $C_i^{m-1,m}$ has fewer points than $\hat{C}_j^{n+1,n}$, the initium of the curve segment $C_i^{m-1,m}$, that is, the dominant point P_i^m, is used to correspond to the left points of the curve segment $\hat{C}_j^{n+1,n}$, in order to continue the calculation in the first item of Eq. (25) until the initium of the curve segment $\hat{C}_j^{n+1,n}$, that is, the dominant point P_j^{n+1}, is reached. A similar calculation is performed in the region R_1.

The digital matching error shown in Eqs. (25)–(29) is performed when the partial curve $\hat{C}_j^{n+1,n-1}$ is rotated from 0° to 360° in steps of δ°. The minimal matching error between the curve segments $C_i^{m-1,m}$ and $\hat{C}_j^{n+1,n}$ can be obtained according to Eq. (19). Section 6 gives the experimental results obtained by using this algorithm.

6. Experiment Results

In this section, we present experimental results for the recovery of connection relationships among two-dimensional objects.

The first experiment employs the image in **Fig. 5**, which includes two objects. The left bottom corner of the input image is the origin of the coordinates. After being binarized, the objects are numbered O_0 and O_1 in order of searching when the boundary-tracing algorithm is applied, and the two closed boundary curves are numbered C_0 and C_1, correspondingly, as shown in **Fig. 6**. The lengths of C_0 and C_1 are 490 and 504 dots, respectively. Therefore, the scale σ ranges from 0 to $\sigma_{\max} = \min\{490, 504\}/6$. The Gaussian-smoothed boundary curves are given in **Fig. 7**, when $\sigma = 82$. The separation points obtained are $S_{P_0} = \{P_0^0, P_0^1, \cdots, P_0^{19}\}$ and $S_{P_1} = \{P_1^0, P_1^1, \cdots, P_1^{19}\}$, which are numbered clockwise and are plotted on the corresponding curve, as shown in **Fig. 8**. LCMCs between the objects O_0 and O_1, whose lengths are greater than L_{thres} (= 3), are shown in **Table 1**, in which LCMCs are listed in such a way that the matching errors are ordered from small to large. The first column shows the number of LCMCs. The second and third columns show the initiums and termini of the partial curves of the object O_0, and the fourth and fifth columns those of the object O_1, respectively. The sixth column shows the lengths of LCMCs, that is, the number of the matched curve segment pairs

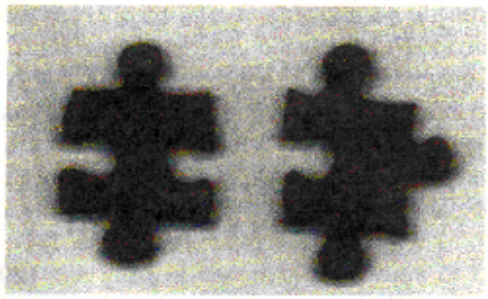

Fig. 5 Input image including two objects.

Fig. 6 Closed boundary curves obtained.

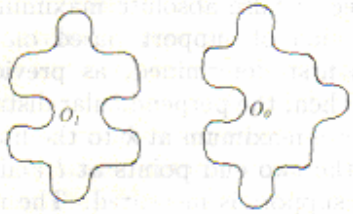

Fig. 7 Gaussian-smoothed boundary curves ($\sigma = 82$).

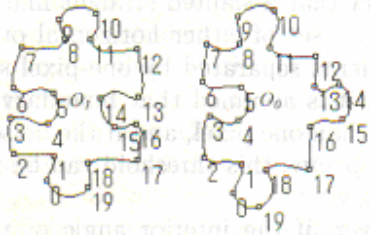

Fig. 8 Separation points marked by small "o" on the original curves.

Table 1 LCMCs between the objects O_0 and O_1 whose lengths are greater than L_{thres}.

LCMC No.	Partial curve of O_0		Partial curve of O_1		LCMC length	Rotation angle of O_1	Matching error
	Initium	Terminus	Initium	Terminus			
1	P_0^{17}	P_0^{0}	P_1^{5}	P_1^{2}	4	-267°	193.47
2	P_0^{2}	P_0^{5}	P_1^{0}	P_1^{17}	4	-91°	260.53
3	P_0^{7}	P_0^{10}	P_1^{15}	P_1^{12}	4	96°	352.15
4	P_0^{4}	P_0^{7}	P_1^{5}	P_1^{2}	4	-183°	491.86
5	P_0^{2}	P_0^{6}	P_1^{17}	P_1^{13}	5	-13°	498.11
6	P_0^{1}	P_0^{5}	P_1^{4}	P_1^{0}	5	-177°	616.20

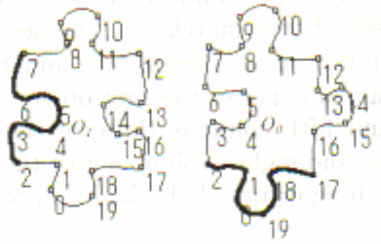

Fig. 9 Connection relationship between the two objects O_0 and O_1, shown by thick curves.

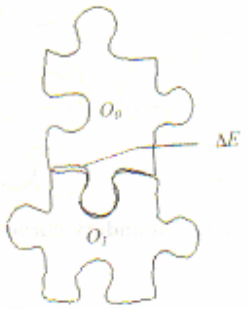

Fig. 10 Recovered relationship between the two objects.

included in LCMCs. The seventh column shows the rotation angle of the partial curves of the object O_1. A negative rotation angle indicates counterclockwise movement, and a positive one clockwise movement. The eighth column show the matching errors of LCMCs, that is, the matching error between the partial curves of the objects O_0 and O_1. Because the first LCMC has the smallest matching error, it is considered that the connection relationship between object O_0 and O_1 exists at this LCMC. As related in Section 4.3, when we say that the curve segment $C_i^{m-1,m}$ matches $\hat{C}_j^{n,n+1}$, we mean that the curve segment pair $C_i^{m-1,m}C_i^{m,m+1}$ matches the curve segment pair $\hat{C}_j^{n+1,n}\hat{C}_j^{n,n-1}$. In this example, the curve segment $C_0^{17,18}$ matches the curve segment $\hat{C}_1^{7,6}$, that is to say, the curve segment pair $C_0^{17,18}C_0^{18,19}$ matches the curve segment pair $\hat{C}_1^{7,6}\hat{C}_1^{6,5}$. Therefore, the LCMC with the smallest matching error comprises the partial curves $C_0^{17,2}$ and $\hat{C}_1^{7,2}$, which are shown by thick curves in **Fig. 9**. The connection relationship recovered on the basis of this LCMC is shown in **Fig. 10** after the object O_1 is translated 136 dots along the X-axis and -73 dots along the Y-axis, and is rotated through 267° counterclockwise.

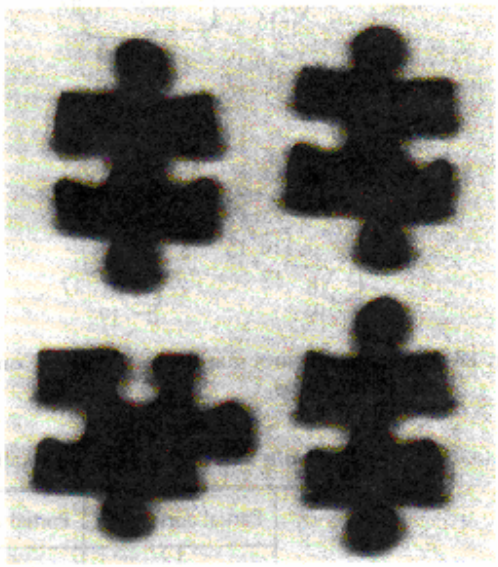

Fig. 11 Input image including four objects.

Another experiment employs the image in **Fig. 11**, which includes four objects. After being binarized, the objects are numbered O_0, O_1, O_2, and O_3, in the order of searching when the boundary-tracing algorithm is applied, as shown in **Fig. 12**. Thus, the object set and boundary set are $S_O = \{O_0, O_1, O_2, O_3\}$ and

$S_C = \{C_0, C_1, C_2, C_3\}$. The separation points obtained are plotted on the corresponding boundary curve and numbered clockwise (see **Fig. 13**). The separation point sets are $S_{P_0} = \{P_0^0, P_0^1, \cdots, P_0^{19}\}$, $S_{P_1} = \{P_1^0, P_1^1, \cdots, P_1^{19}\}$, $S_{P_2} = \{P_2^0, P_2^1, \cdots, P_2^{19}\}$, and $S_{P_3} = \{P_3^0, P_3^1, \cdots, P_3^{19}\}$. The four curves in S_C are, respectively, broken into four sets of curve segments at these four sets of separation points, which are $S_{C_0} = \{C_0^{0,1}, C_0^{1,2}, \cdots, C_0^{18,19}, C_0^{19,0}\}$, $S_{C_1} = \{C_1^{0,1}, C_1^{1,2}, \cdots, C_1^{18,19}, C_1^{19,0}\}$, $S_{C_2} = \{C_2^{0,1}, C_2^{1,2}, \cdots, C_2^{18,19}, C_2^{19,0}\}$, and $S_{C_3} = \{C_3^{0,1}, C_3^{1,2}, \cdots, C_3^{18,19}, C_3^{19,0}\}$, when traced clockwise. The curve segments in these four sets are matched with each other. The LCMCs with the smallest matching error between every two different objects are listed in **Table 2**, and are shown by thick corresponding curves in **Fig. 14**. The first column of Table 2 shows the two objects being matched. The second and third columns show the initium and terminus of the partial curve of the first object, and the fourth and fifth columns those of the second. The sixth and eighth columns give the lengths and matching errors of the LCMCs, while sev-

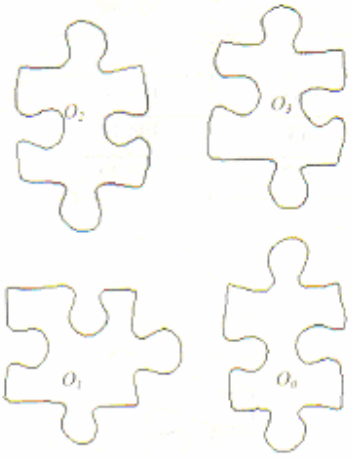

Fig. 12 Closed boundary curves obtained.

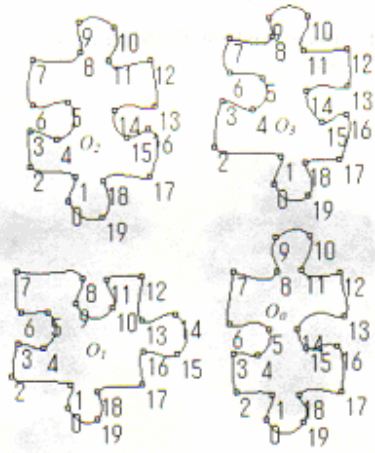

Fig. 13 Separatin points marked by small "o" on the original curves.

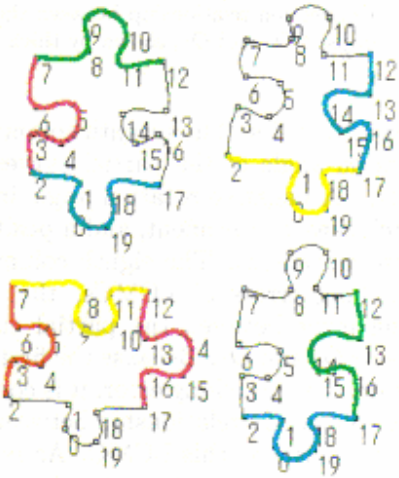

Fig. 14 LCMCs between every two objects.

Table 2 LCMCs with the smallest matching errors between every two objects.

O_i-O_j	Partial curve of O_i		Partial curve of O_j		LCMC	Rotation	Matching
	Initium	Terminus	Initium	Terminus	length	angle of O_j	error
O_0-O_1	P_0^{17}	P_0^0	P_1^5	P_1^2	4	-272°	131.15
O_0-O_2	P_0^{12}	P_0^{15}	P_2^{10}	P_2^7	4	268°	178.62
O_0-O_3	P_0^{17}	P_0^0	P_3^{15}	P_3^{12}	4	-93°	211.55
O_1-O_2	P_1^{12}	P_1^{15}	P_2^5	P_2^2	4	0°	211.00
O_1-O_3	P_1^7	P_1^{10}	P_3^0	P_3^{17}	4	-2°	161.93
O_2-O_3	P_2^{17}	P_2^0	P_3^{15}	P_3^{12}	4	-89°	283.78

enth shows the rotation angle of the second object.

It is worth noting that not all LCMCs for which connection relationships exist are correct. For example, the LCMCs in the second and fourth row are contradictory, because a partial curve of an object cannot be connected with two partial curves of two different objects. To recover the connection relationships among these objects, the contradictory LCMCs that should not be used in connection relationship recovery must be detected beforehand. The contradictory LCMCs are determined according to the two rules given in Section 4.5. Since *Rule* 1 has higher priority, it is used first. Through application of *Rule* 1, the LCMCs in the second and fourth rows of Table 2 are considered to be contradictory, and are discarded. Then, through application of *Rule* 2 to the remaining LCMCs in Table 2, the LCMC in the seventh row is considered to be contradictory and is discarded. It is worth noting that LCMCs remain in rows 3, 5 and 6 of Table 2 at this point. The numbers of matched partial curves of objects 1 and 2 are both two, but the sum of the matching errors between object 1 and 2 and objects 1 and 3, is smaller than that of matching errors between objects 2 and 0 and objects 2 and 1, and therefore object O_1 is selected as the base object from which the recovery of the connection relationship is started.

In the first step, the connection relationship between objects O_1 and O_2, and objects O_1 and O_3, are recovered, because objects O_2 and O_3 can be connected to the base object O_1 directly. The translations of object O_2 along the X-axis and Y-axis are 79 dots and -150 dots, and the rotation angle is 0 degrees. These three parameters of object O_3 are -141 dots, -83 dots, and -2 degrees, correspondingly.

In the second step, the connection relationship between object O_0 and the composite object obtained above is recovered. The translations along the X-axis and Y-axis of object O_0 are -63 dots and 70 dots, and the rotation angle is -268 degrees, which is the sum of the rotation angles of object O_0 to the object O_2 ($-268°$) and object O_2 to O_1 ($+0°$). Note that the rotation angle in row 3 and column 7 of Table 2 is the rotation angle of object 2 to object 0. The final recovery result of this experiment is shown in **Fig. 15**.

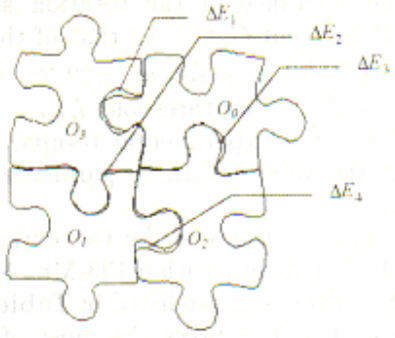

Fig. 15 Recovered relationship among the objects.

7. Conclusions and Discussions

This paper has discussed the recovery of connection relationships among two-dimensional objects. The results of experiments performed with real-world images showed the validity of our method for recovering such relationships. The method can be applied to intelligent robot assembly systems.

In the method, a closed boundary curve is first broken into a set of curve segments at the separation points at which the absolute curvature has local maxima. Then, the curve segments are matched with those in another set belonging to another object, and LCMCs are detected. The connection relationship is determined on the basis of these LCMCs. One important consideration in this method is whether the segmentation of the boundary curve can be performed stably; that is to say, whether the separation points can be detected stably. Fortunately, many methods for detecting dominant points have been proposed. Among these methods, multiscale-based dominant point detection is known to be the most stable, most reliable, and most resistant to the effects of noise[15]. Therefore, we employed this method to detect the dominant points. The scale σ ranges from 0 to $\sigma_{\max} = S/6$. By changing the scale level σ, we can obtain the desirable dominant points.

We set three conditions for detecting LCMCs. Because the threshold E_{thres} depends on the lengths of the curve segments, it is decided dynamically. The weighting coefficient W_E is determined experimentally, and was set at 0.238 in our two experiments. Since the slants of the two continuous curve segments $\hat{C}_j^{n+1,n}$ and $\hat{C}_j^{n,n-1}$, in which the matching errors between the curve segments $C_i^{m-1,m}$ and $\hat{C}_j^{n+1,n}$, and $C_i^{m,m+1}$ and $\hat{C}_j^{n,n-1}$ are minimal, are not iden-

tical, the tolerance of the rotation angle of the curve segment $\hat{C}_j^{n,n-1}$ to that of the curve segment $\hat{C}_j^{n+1,n}$ was set at $\pm 22.5°$, that is, $\Delta\theta_{thres} = 45°$. The threshold L_{thres} was set at 3. From the experimental results, we can say that the values of these parameters were appropriate.

The execution times of the two experiments on a DOS/V machine with a 133-Mhz Pentium Over Drive Processor are listed in **Table 3**. We can see that step 2 takes the most of execution time, and that the time for curve segmentation is negligible in comparison with that of curve segment matching. Therefore the execution time for step 2 can be given by

$$T_{step2} = crO((N-1)! \times D_{\max 1} \times D_{\max 2}), \tag{30}$$

Table 3 Execution time of every step (unit: ms).

	Contents of processing	Ex. 1	Ex. 2
Step 1	Boundary curve tracing	165	220
	Convolution with Gaussian smoothing function	879	1922
	Curvature calculation and dominant points detection	165	275
Step 2	Curve segmentation and curve segment matching	894069	5528256
Step 3	Determination the connection relationship	5767	15599
	Recovery of the connection relationship	55	55
Total		901100	5546327

where N is the total number of the objects in the input image, $D_{\max 1}$ and $D_{\max 2}$ are the largest and second largest numbers of separation points, that is, $D_{\max 1} = \max\{D_0, D_1, \cdots, D_{N-1}\}$, $D_{\max 2} = \max\{D_0, D_1, \cdots, D_{N-1}\} - \{D_{\max 1}\}$. The coefficient r is the time needed for matching between the longest and the second longest partial curves in $\{S_{C_0}, S_{C_1}, \cdots, S_{C_{N-1}}\}$. The coefficient c is the number of rotation times in the range 0°–360°, and is determined by $360/\delta$. The execution time T_{step2} is heavily influenced by the value of δ, which is the amount by which the rotation angle is incremented during one rotation operation. In these two experiments, δ is set at 1°.

The minimal matching errors between the curve segments $C_0^{17,18}$, $C_0^{18,19}$, $C_0^{19,0}$, $C_0^{0,1}$, and $C_0^{1,2}$ (shown by A–E) of object O_0 and all curve segments of object O_1 in the first experiment are shown in **Fig. 16**. Their rotation angles corresponding to these minimal matching errors are given in **Fig. 17**. The horizontal double-dotted-and-dashed line in Fig. 16 shows the position of E_{thres}, while the vertical dotted lines in Fig. 16 and Fig. 17 indicate the position of the LCMC with the minimal matching error. The range of tolerance of the rotation angles of the curve segments of this LCMC is shown by two horizontal double-dotted-and-dashed lines in Fig. 17. From these results, we can say that the method for determining the threshold E_{thres} and the three conditions for detecting LCMCs are appropriate.

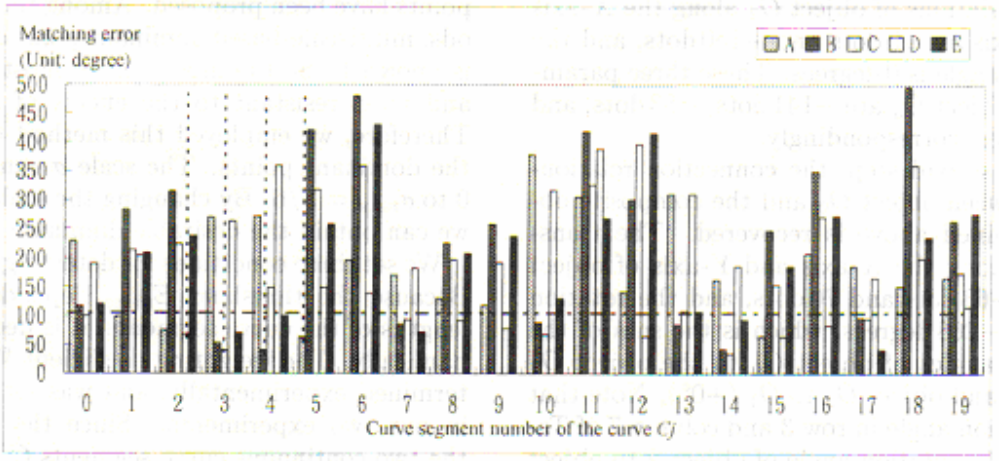

Fig. 16 Matching errors between the curve segments 17–19, 0–1 (shown by *A*–*E*) of the object on the right and all curve segments of the object on the left in Fig. 5.

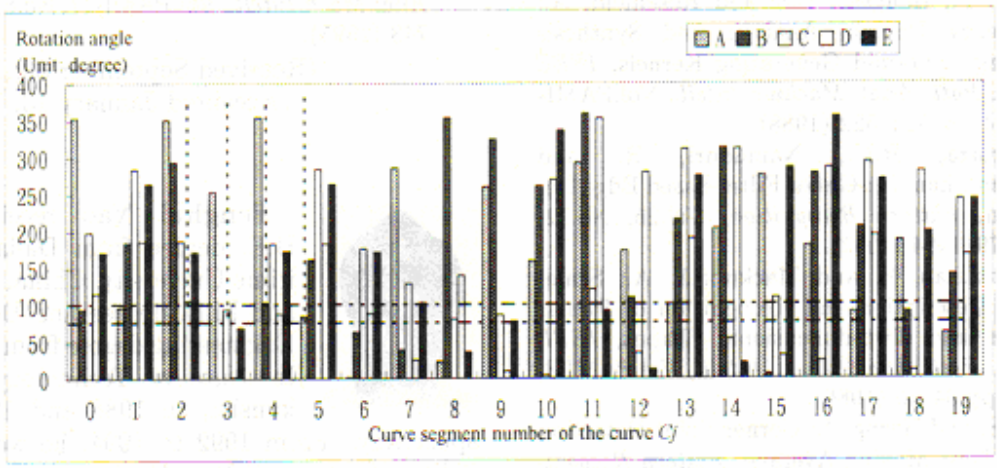

Fig. 17 Rotation angles of all curve segments of the object on left when it is matched with curve segments 17–19, 0–1 (shown by A–E) of the object on the right in Fig. 5.

The gaps in Fig. 10 (represented by ΔE) and in Fig. 15 (shown by ΔE_1, ΔE_2, ΔE_3, and ΔE_4) are errors in the recovery of the connection relationship. There are two factors causing these errors. First, because the image is scanned from top to bottom, the brightness of the edges on the top and bottom sides are different, and there are shadows on the bottom side (see Fig. 5 and Fig. 11). This gives rise to the deformation of boundary curves. Second, the amount by which the rotation angle is incremented in partial curve matching (refer to Section 4.3) is δ. One way of reducing these errors is to select a smaller δ, and the other is to improve the image input environment and the algorithms for binarization and boundary curve detection.

This experiment used the images of objects without any texture. If the objects have textures, boundary curve detection will become more difficult. Moreover, partial curve matching will have to be performed between every two pairs of curve segments belonging to two different objects, which will be very time-consuming. In our experiment, if a partial curve of an object matches the partial curves of multiple objects, these matched curves are discarded. In fact, it is necessary, in this case, to employ the image values near the matched curves to find the optimally matched partial curve. These problems are left to be solved in the future.

Acknowledgments The authors greatly appreciate the valuable suggestions and comments of the anonymous reviewers.

References

1) Anderson, I.M. and Bezdek, J.C.: Curvature and Tangential Deflection of Discrete Arcs: A Theory Based on the Commutator of Scatter Matrix Pairs and Its Application to Vertex Detection in Planar Shape, *IEEE Trans. Patt. Anal. Mach. Intell.*, Vol.PAMI-6, No.1, pp.27–40 (1984).
2) Bergholm, F.: Edge Focusing, *IEEE Trans. Patt. Anal. Mach. Intell.*, Vol.PAMI-9, No.6, pp.726–741 (1987).
3) Burt, P.J.: Fast Filter Transforms for Image Processing, *Comput. Vision, Graphics & Image Processing*, Vol.16, pp.20–51 (1981).
4) Burt, P.J. and Adelson, E.H.: The Laplacian Pyramid as a Compact Image Code, *IEEE Trans. Commun.*, Vol.COM-31, No.4 (1983).
5) Canny, J.F.: A Computational Approach to Edge Detection, *IEEE Trans. Patt. Anal. Mach. Intell.*, Vol.PAMI-8, No.6, pp.679–698 (1986).
6) Freeman, H. and Davis, L.S.: A Corner-finding Algorithm for Chain-coded Curves, *IEEE Trans. Comput.*, Vol.C-26, pp.297–303 (1977).
7) Freeman, H. and Garder, L.: A Pictorial Jigsaw Puzzles: The Computer Solution of a Problem in Pattern Recognition, *IEEE Trans. Electronic Comput.*, Vol.EC-13, pp.118–127 (1964).
8) Haralick, R.M.: Digital Step Edges from Zero Crossing of Second Directional Derivatives, *IEEE Trans. Patt. Anal. Mach. Intell.*, Vol.PAMI-6, No.1, pp.58–68 (1984).
9) Marr, D.C. and Hildreth, E.: Theory of Edge Detection, *Proc. Roy. Soc. London*, Vol.B207, pp.187–217 (1980).

10) Meer, P., Baugher, E.S. and Rosenfeld, A.: Frequency Domain Analysis and Synthesis of Image Pyramid Generating Kernels, *IEEE Trans. Patt. Anal. Machine Intell.*, Vol.PAMI-9, No.4, pp.512–522 (1988).
11) Mehrotra, R.K., Namuduri, R. and Ranganathan, N.: Gabor Filter-based Edge Detection, *Pattern Recognition*, Vol.25, No.12, pp.1479–1494 (1992).
12) Mokhtarian, F. and Mackworth, A.: Scale-based Description and Recognition of Planar Curves and Two-dimensional Shapes, *IEEE Trans. Patt. Anal. Mach. Intell.*, Vol.PAMI-8, No.1, pp.34–43 (1986).
13) Pei, S. and Horng, J.: Corner Point Detection Using Nest Moving Average, *Pattern Recognition*, Vol.27, No.11, pp.533–1537 (1994).
14) Persoon, E. and Fu, K.: Shape Discrimination Using Fourier Descriptors, *IEEE Trans. Systems, Man, Cybern.*, Vol.SMC-7, No.3, pp.170–179 (1977).
15) Rattarangsi, A. and Chin, R.T.: Scale-based Detection of Corners of Planar Curves, *IEEE Trans. Patt. Anal. Mach. Intell.*, Vol.PAMI-14, No.4, pp.432–449 (1992).
16) Rosenfeld, A. and Thurston, M.: Edge and Curve Detection for Visual Scene Analysis, *IEEE Trans. Comput.*, Vol.C-20, No.5, pp.562–569 (1971).
17) Rosenfeld, A. and Johnston, E.: Angle Detection on Digital Curves, *IEEE Trans. Comput.*, Vol.C-22, pp.875–878 (1973).
18) Rosenfeld, A. and Weazka, J.S.: An Improved Method of Angle Detection on Digital Curves, *IEEE Trans. Comput.*, Vol.C-24, pp.940–941 (1975).
19) Sekita, I., Kurita, T. and Otsu, N.: Complex Autoregressive Model for Shape Recognition, *IEEE Trans. Patt. Anal. Mach. Intell.*, Vol.PAMI-14, No.4, pp.489–496 (1992).
20) Teh, C. and Chin, R.T.: On the Detection of Dominant Points on Digital Curves, *IEEE Trans. Patt. Anal. Mach. Intell.*, Vol.PAMI-11, No.8, pp.859–872 (1989).
21) Yao, F., Shao, G., Tamaki, A. and Kato, K.: Partial Curve Identification in 2-D Space and Its Application to Robot Assembly, *Proc. 3rd International Workshop on Image and Signal Processing Advances in Computational Intelligence*, Manchester, Nov. 4–7, pp.161–164 (1996).
22) Yuille, A.L. and Poggio, T.A.: Scaling Theorems for Zero-crossing, *IEEE Trans. Patt. Anal. Mach. Intell.*, Vol.PAMI-8, No.1, pp.15–25 (1986).
23) Zhu, P. and Chirlian, P.M.: On Critical Point Detection of Digital Shapes, *IEEE Trans. Patt. Anal.Mach.Intell.*, Vol.PAMI-17, No.8, pp.737–748 (1995).

(Received September 30, 1996)
(Accepted January 10, 1997)

Fenghui Yao received his B.E. degree from Dalian Maritime University, China, in 1984, and M.E. degree and Doctor of Engineering degree from Kyushu Institute of Technology, Kitakyushu, in 1988 and 1992, respectively. From 1992 to 1994, he worked at Soliton Systems K.K.. He is presently a research associate in Department of Electric, Electronic, and Computer Engineering, Kyushu Institute of Technology. His current research interests are image processing, multimedia information processing, computer architecture, and parallel processing. He is a member of IEEE, IPSJ, and IEICE.

Guifeng Shao received her B.E. degree from Wuhan University of Technology on Surveying and Mapping, China, in 1986, and M.E. degree and Doctor of Engineering degree from Kyushu Institute of Technology, Kitakyushu, in 1991 and 1995, respectively. She is currently an associate professor at Department of Commercial Science, Seinan Gakuin University, Fukuoka. Her research interests are natural language understanding and knowledge representation.

Akikazu Tamaki received his B.E. and M.E. degrees from Kyushu Institute of Technology, Kitakyushu, in 1969 and 1971, respectively. He joined the Faculty of Engineering, Kyushu Institute of Technology, Kitakyushu, in 1971, and he is currently a lecturer at Department of Electric, Electronic, and Computer Engineering. His present research interests are computer vision, neural network, and computer music. He is a member of IEEE, IPSJ, ACM, IEICE, BMFSA, and so on.

Kiyoshi Kato received his B.S. and M.S. degrees from Tokyo University in 1959 and 1961, respectively. He received a Doctor of Engineering degree from Tokyo University in 1975. He joined the Faculty of Engineering, Kyushu Institute of Technology, Kitakyushu, in 1964. He is currently a professor at Department of Electric, Electronic, and Computer Engineering. His research interests include image processing, computer application in music and education, and human interfaces. He is a member of IPSJ, IEICE, SICE, and Robotics Society.